PHYSICAL REVIEW E **99**, 052216 (2019)

Lateral inhibition provides a unifying framework for spatiotemporal pattern formation in media comprising relaxation oscillators

R. Janaki,[1,2] Shakti N. Menon,[1] Rajeev Singh,[1,3] and Sitabhra Sinha[1,4]
[1] *The Institute of Mathematical Sciences, CIT Campus, Taramani, Chennai 600113, India*
[2] *Department of Theoretical Physics, University of Madras, Guindy Campus, Chennai 600025, India*
[3] *Department of Physics, Indian Institute of Technology (BHU), Varanasi 221005, India*
[4] *Homi Bhabha National Institute, Anushaktinagar, Mumbai 400094, India*

(Received 12 February 2019; revised manuscript received 26 April 2019; published 23 May 2019)

Differential excitatory and inhibitory interactions, specifically lateral inhibition, between the constituent elements of complex systems underlie a wide range of spatiotemporal patterns in nature. Here, we show that when systems of relaxation oscillators, whose dynamics involve widely separate timescales, are coupled primarily through diffusion of the inactivation component, they exhibit strikingly similar patterns regardless of specific details of the model kinetics and spatial topology. This universality stems from the fact that all observed patterns can be viewed as either specific manifestations of, or arising through interactions between, two fundamental classes of collective dynamics, viz., a state comprising clusters of synchronized oscillators, and a time-invariant spatially inhomogeneous state resulting from oscillator death. Our work provides an unifying framework for understanding the emergent global behavior of various chemical, biological, and ecological systems spanning several time and length scales.

DOI: 10.1103/PhysRevE.99.052216

I. INTRODUCTION

The ubiquity of patterns in nature has, for several decades, stimulated efforts at understanding possible mechanisms that underlie their emergence [1–3]. Such patterns can be manifested in both space and time, with perhaps the most widespread instance of the latter being provided by systems that exhibit relaxation oscillations (see, e.g., Refs. [4–7]). In the simplest scenarios, these can be understood as resulting from interactions between an activator component and an inhibitory (or inactivation) component that operate at fast and slow timescales, respectively [8]. Such oscillators can, in turn, interact with each other, which can result in nontrivial emergent collective dynamics in systems ranging from the cell to the food web [9,10]. As competition between neighboring elements is a recurring motif in such systems, it is natural to consider the consequences of lateral inhibition [11–14] in systems of relaxation oscillators.

In this paper we have explored the collective dynamics in a variety of models arising in chemical, biological, and ecological contexts. The common thread connecting these diverse systems is that all of them are described by systems of relaxation oscillators coupled to their neighbors through the diffusion of their inactivation components. This may, for instance, arise in spatially extended ecological habitats comprising several patches, with each exhibiting oscillations in predator and prey populations, where only the predator (acting as the inactivation component) can move across neighboring patches, e.g., as in herbivore-vegetation interactions [15]. Experimental realizations of such systems involving oscillating chemical reactions in microfluidic devices have demonstrated the existence of several striking patterns [16]. These include antiphase synchronization, as well as spatially heterogeneous time-invariant patterns. While the latter resemble stripes generated by the Turing mechanism [17], it has been analytically demonstrated using a generic model that these result from spatially patterned oscillation death [18]. Here, we show that the patterns seen in these systems can arise in much more general contexts, specifically involving models characterized by different local dynamics and connection topologies, and which describe processes across a wide range of spatial scales. Such "universality" arises from the fact that the patterns generated by such systems are either specific manifestations of, or arise through interactions between, two basic classes of patterns. Moreover, these fundamental patterns should be observable in any system where lateral inhibition couples oscillators whose dynamics is governed by interactions between components characterized by widely separate timescales.

II. THE MODEL

The dynamical behavior of a spatially extended system of N relaxation oscillators (each comprising R variables) that interact over a general connection topology can be described by the coupled system of equations:

$$\frac{dx_i^{(p)}}{dt} = \mathcal{F}_{(p)}\big(x_i^{(1)}, x_i^{(2)}, \ldots, x_i^{(R)}\big) + D_{(p)} \sum_{j \in S_i} \frac{x_j^{(p)} - x_i^{(p)}}{k_i}, \tag{1}$$

where $x_i^{(p)}$ $(i = 1, 2, \ldots, N,\ p = 1, 2, \ldots, R)$ represents the pth component of the ith oscillator. The dynamics of an uncoupled node is specified by the functions $\mathcal{F}_{(p)}$ and governed by parameters whose values are chosen so as to yield oscillations. The diffusion terms represent the interactions

2470-0045/2019/99(5)/052216(9)

of each node i with its k_i neighbors (comprising the set S_i) through the different components $x^{(p)}$ with coupling strengths $D_{(p)}$. The net contribution that each node receives through these diffusive interactions is normalized by the number of its neighbors k_i, so as to make the results comparable across systems with different connection topologies. For systems of oscillators that are coupled over regular lattices with periodic boundary conditions, each node has a fixed number of neighbors, e.g., $k_i = 2$ for a ring and $k_i = 4$ for a square lattice. The same framework can also be applied to networks of oscillators having arbitrary connection topology, where k_i may vary across nodes.

With the exception of one of the models (viz., the cell-cycle model, described below in Sec. II A), the individual oscillators that we have considered are described by only two components (u and v, say) that are responsible for activation and inhibition, respectively. These systems can hence be described by the equations

$$\frac{du_i}{dt} = \mathcal{F}_u(u_i, v_i) + D_u \sum_{j\in S_i} \frac{u_j - u_i}{k_i},$$
$$\frac{dv_i}{dt} = \mathcal{F}_v(u_i, v_i) + D_v \sum_{j\in S_i} \frac{v_j - v_i}{k_i}, \tag{2}$$

where u_i and v_i ($i = 1, 2, \ldots N$) represent the activation and inactivation components, respectively. In this paper we focus on spatiotemporal patterns seen in systems possessing simple regular geometries, viz., one-dimensional (1D) and two-dimensional (2D) lattices. Motivated by examples of lateral inhibition in nature, where communication between neighboring regions occurs almost exclusively through the inactivation component (such as the ones mentioned earlier), we consider the case $D_u = 0$ for all simulations reported here (unless mentioned otherwise). We have explicitly verified that qualitatively similar results are obtained even when this constraint is relaxed (e.g., when $D_u = D_v$), provided the kinetics of the inactivation component is sufficiently slower than that of the activation component. We would also like to point out that when the coupling is exclusively through diffusion of the activation variable (i.e., $D_v = 0$), the collective dynamics does not display the wide variety of patterns obtained in the current investigation and exhibits only synchronized oscillations (Fig. 1). For most results reported here, $N = 20$ (for 1D) and $N \times N = 60^2$ (for 2D), although we have used other values of N to verify that our results are not sensitively dependent on system size. The boundary conditions are taken to be periodic to minimize boundary effects. The equations are solved using a variable step stiff solver. Time units in each case are normalized with respect to the time period of an uncoupled oscillator for the corresponding set of parameter values. In the following subsections we describe in detail each of the four models, characterized by different choices of the functional forms for $\mathcal{F}$, and whose collective dynamics we investigate. Spatiotemporal evolution (for one-dimensional arrays) and snapshots (for two-dimensional lattices) of the activation patterns for the different models are shown in Figs. 2(a)–2(d), while Figs. 3(a)–3(h) indicate the different types of dynamical behavior observed in these models by varying the parameter values.

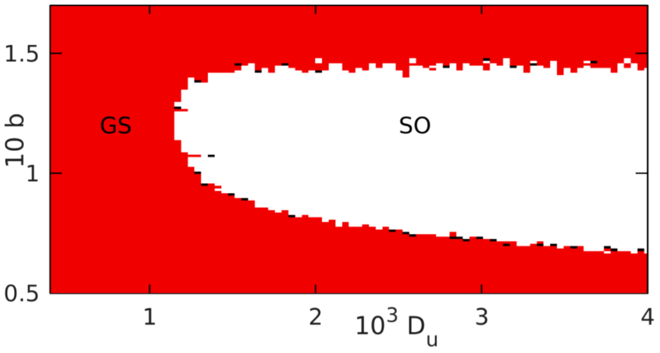

FIG. 1. The collective dynamics of a ring of $N = 20$ oscillators, described by the FitzHugh-Nagumo model (FHN), that are diffusively coupled through the activator component u alone (i.e., $D_v = 0$). The (D_u, b) parameter plane, where D_u represents the coupling strength between activator components of the neighboring oscillators and b is a measure of the asymmetry of the oscillators, shows that the dynamics of the system converges either to gradient synchronization (GS) or synchronized oscillation (SO) attractors.

A. Cell-cycle model

In the first system that we consider, the individual oscillators describe the cell cycle, i.e., the periodic sequence of events in a cell resulting in it dividing into two daughter cells. The oscillator description used here is adapted from a three-component model for early embryogenesis in *Xenopus laevis*, developed by Ferrell *et al.* [19], which involves interactions between the proteins CDK1, Plk1, and APC. Over the course of the cell cycle, CDK1 activates Plk1, which in turn activates the protein APC that subsequently suppresses CDK1.

Representing the concentrations of CDK1, Plk1, and APC by u, v, and w, respectively, the time-evolution of this system is governed by Eq. (1) with the functions $\mathcal{F}_u$, $\mathcal{F}_v$, and $\mathcal{F}_w$ described by

$$\mathcal{F}_u(u, v, w) = \alpha_1 - \beta_1 u\left(\frac{w^{n_1}}{k_1^{n_1} + w^{n_1}}\right) + \alpha_4\,(1-u)\left(\frac{u^{n_4}}{k_4^{n_4} + u^{n_4}}\right),$$
$$\mathcal{F}_v(u, v, w) = \alpha_2\,(1-v)\left(\frac{u^{n_2}}{k_2^{n_2} + u^{n_2}}\right) - \beta_2\, v,$$
$$\mathcal{F}_w(u, v, w) = \alpha_3\,(1-w)\left(\frac{v^{n_3}}{k_3^{n_3} + v^{n_3}}\right) - \beta_3\, w. \tag{3}$$

Note that the positive and negative feedback loops make each of the uncoupled elements a relaxation oscillator with distinct fast and slow phases. Typical values of the model parameters that generate oscillations are $\alpha_1 = 0.02, \alpha_2 = 3, \alpha_3 = 3, \alpha_4 = 3, \beta_1 = 3, \beta_2 = 1, \beta_3 = 1, k_1 = 0.5, k_2 = 0.5, k_3 = 0.5, k_4 = 0.5, n_1 = 8, n_2 = 8, n_3 = 8$, and $n_4 = 8$.

As APC is a relatively large regulatory complex, one may consider interactions through the diffusion of this protein to be negligible. We use the fact that Plk1 indirectly suppresses CDK1 by activating APC, to consider its concentration as the inactivation variable in our simulations. We have therefore considered only diffusive coupling through the variable v (i.e., $D_u = D_w = 0$). The patterns shown in Fig. 2(a) are obtained

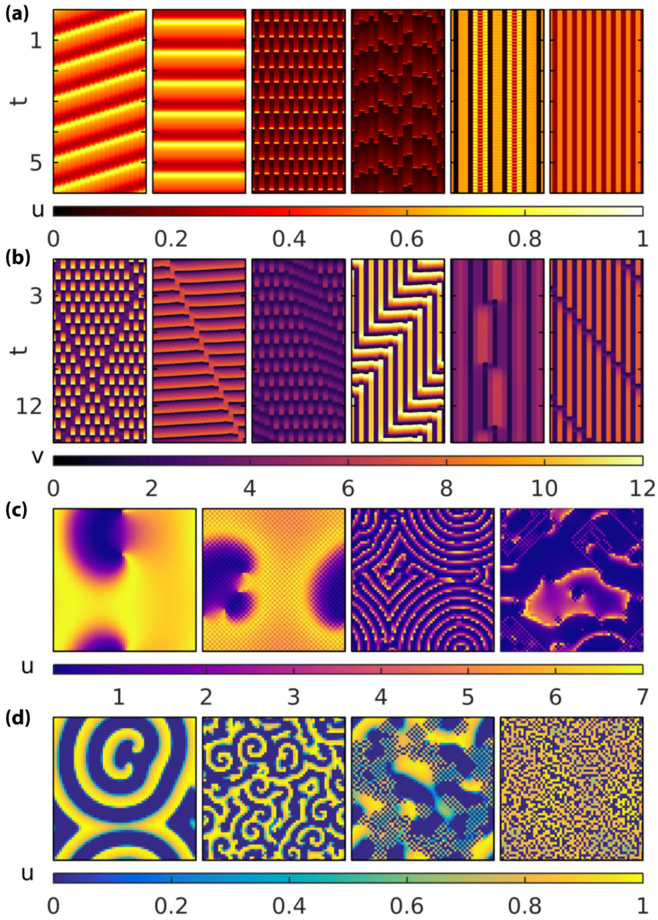

FIG. 2. Diversity of complex spatiotemporal patterns observed in several systems described by lattices of relaxation oscillators, coupled through diffusion of their inactivation variables. (a, b) Pseudocolor representation of the spatiotemporal evolution of the activation variable u for one-dimensional arrays of oscillators described by (a) a cell cycle model adapted from Ferrell *et al.* [19] and (b) the Brusselator model for autocatalytic chemical reactions [20]. Both systems comprise $N = 20$ oscillators arranged on a ring. Attractors of the spatiotemporal dynamics of the system shown in (a) include (L-R) gradient synchronization (GS), synchronized oscillations (SO, a special case of GS), antiphase synchronization (APS), a pattern exhibiting generalized synchronization, chimera state (CS) characterized by coexistence of oscillating and nonoscillating elements, and spatially patterned oscillation death (SPOD) state. Other complex patterns in addition to those mentioned above emerge from the spatiotemporal evolution of the system of coupled chemical oscillators shown in (b). Snapshots of the activation variable u in a two dimensional array (with periodic boundary conditions) comprising $N \times N$ relaxation oscillators described by (c) the Brusselator model and (d) the Rosenzweig Macarthur model of predator-prey dynamics [15]. For both systems, $N = 60$ with each oscillator coupled to their four nearest neighbors. The patterns seen in (c) include (L-R) GS and generalized APS, both exhibiting spiral waves, a tightly wound spiral representing a complex phase relationship between the oscillators and CS (checkerboard regions comprise nonoscillating nodes). Similar patterns are seen in (d), viz., (L-R) single and multiple spirals, CS, and SPOD.

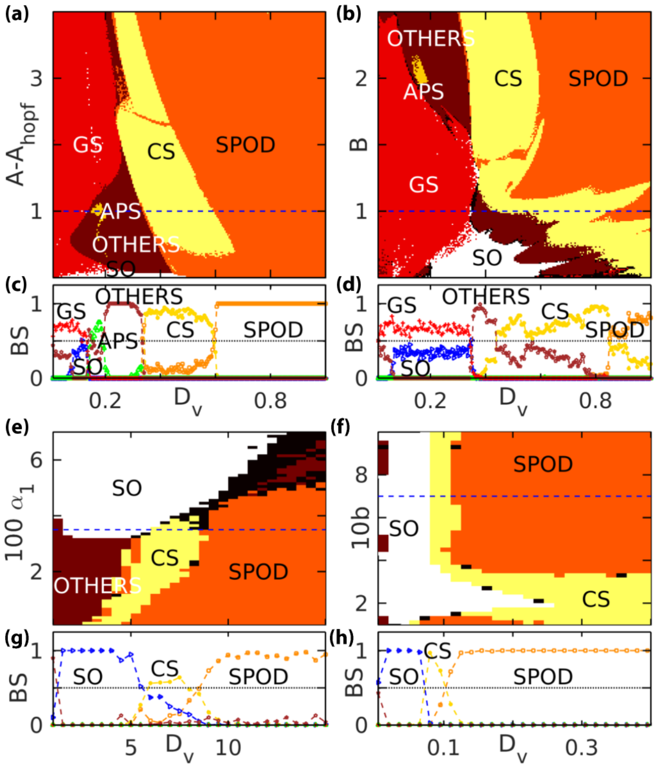

FIG. 3. The distinct collective dynamics observed in different regions of the parameter space for arrays of relaxation oscillators diffusively coupled through the inactivation variable, where each oscillator is described by the Brusselator (a–d), cell-cycle (e, g), or Rosenzweig-MacArthur (f, h) models. (a, b) Different dynamical regimes for a ring of oscillators described by the Brusselator model, shown in the (D_v, $A - A_{\rm hopf}$) and (D_v, B) parameter planes respectively. The regimes are labeled by the attractor to which the majority ($> 50\%$) of initial conditions converge, viz., SO, GS, APS, CS, and SPOD, as well as a variety of other patterns that are referred together as OTHERS. For both panels $N = 40$, with $B = 2$ for panel (a) and $A - A_{\rm hopf} = 1$ for panel (b). At $A = A_{\rm hopf} (= 1 + B^2)$, an uncoupled element undergoes a Hopf bifurcation. (c, d) Multistability of different regimes is indicated by the variation of the basin sizes (BS) for each attractor as D_v is varied along the broken lines in panels (a) and (b), respectively (BS is defined as the fraction of initial conditions that converge to a particular dynamical attractor). (e) Parameter space diagram for a ring of $N = 20$ oscillators described by the cell-cycle model, shown along the (D_v, α_1) plane. (f) Collective dynamical states of a two-dimensional lattice of $N \times N$ ($N = 10$) oscillators described by the Rosenzweig-MacArthur prey-predator model, shown along the (D_v, b) plane. (g, h) Coexistence of multiple regimes at different parameter values is manifested in the BS of these regimes shown as a function of D_v along the broken lines in panels (e) and (f), respectively.

by varying the model parameters α_1, α_2, β_1 and the coupling strength D_v. A detailed parameter phase diagram is shown in Fig. 3(e). The sizes of the basins of attraction for the different dynamical regimes obtained when D_v is varied along the broken line in Fig. 3(e) are displayed in Fig. 3(g).

B. Brusselator chemical oscillator model

The next system we consider consists of oscillators that describe the far-from-equilibrium behavior of chemical systems in which the concentrations of some reactants exhibit periodic variations. The specific model used is the *Brusselator* [20], a simplified description of autocatalytic chemical reactions, such as those belonging to the Belousov-Zhabotinsky (BZ) class of reactions [21]. Representing the activator and inhibitor by u and v respectively, the time evolution of the system is described by Eq. (2) with the functions $\mathcal{F}_u$ and $\mathcal{F}_v$ described by

$$\begin{aligned}\mathcal{F}_u(u,v) &= B + u^2\,v - (1+A)\,u,\\ \mathcal{F}_v(u,v) &= A\,u - u^2\,v,\end{aligned} \tag{4}$$

where A, B are parameters whose values can be appropriately chosen to make the system oscillate. For our simulations, we consider $A > A_{\text{hopf}} (= 1 + B^2)$, where A_{hopf} is the value of A at which a Hopf bifurcation occurs. Motivated by recent experiments on coupled chemical oscillators in microfluidic devices [16], where beads containing the BZ reactive solution are suspended in a chemically inert medium that allows passage of only the inhibitory chemical species, we have considered $D_u = 0$. Figs. 2(b) and 2(c) shows the different patterns that are obtained by varying the values of the parameters A, B, and D_v and detailed parameter phase diagrams are shown in Figs. 3(a) and 3(b). The sizes of the basins of attraction for the different dynamical regimes as a function of D_v along the broken lines in Figs. 3(a) and 3(b) are shown in Figs. 3(c) and 3(d), respectively.

C. Rosenzweig-MacArthur predator-prey model

We next consider a model system whose individual oscillators describe the dynamics arising from interactions between populations of prey (described by the fast activation variable u) and predator species (described by the slow inactivation variable v). The specific form for the functions $\mathcal{F}_u$ and $\mathcal{F}_v$ are obtained from the Rosenzweig-MacArthur model [15,22], viz.,

$$\begin{aligned}\mathcal{F}_u(u,v) &= r\,u\Big(1-\frac{u}{K}\Big) - q\,\frac{u}{b+u}\,v,\\ \mathcal{F}_v(u,v) &= \epsilon\,q\,\frac{u}{b+u}\,v - d\,v,\end{aligned} \tag{5}$$

where r is the intrinsic growth rate, K is the carrying capacity of the prey population, q is the maximum predation rate of the predator, b is the half saturation constant and ϵ and d represent the efficiency and the death rate of the predator, respectively. For our simulations, we have set $r = 1$, $K = 1$, $q = 2$, $d = 0.1$ $b = 0.1$ and $\epsilon = 0.1$. At $K = K_{\text{hopf}}[= b(\epsilon q + d)/(\epsilon q - d)]$, an uncoupled element undergoes a Hopf bifurcation. There are many trophic interactions in which the prey is immobile (e.g., vegetation) and the predator is able to graze by moving from one patch to another (e.g., herbivore). In such a context, one can set $D_u = 0$ and vary D_v. Figure 2(d) shows the different patterns that are obtained on varying D_v. A detailed parameter phase diagram is shown in Fig. 3(f). The sizes of the basins of attraction for the different dynamical regimes obtained as D_v is varied along the broken line in Fig. 3(f) are shown in Fig. 3(h).

D. FitzHugh-Nagumo model

For the bulk of our simulations, we have considered perhaps the most generic model of relaxation oscillators, viz., the FitzHugh-Nagumo (FHN) model [23]. Here, each oscillator is described by a fast activation variable u and a slow inactivation variable v. The time-evolution of this model is governed by the functions

$$\begin{aligned}\mathcal{F}_u(u,v) &= u(1-u)(u-\alpha) - v,\\ \mathcal{F}_v(u,v) &= \epsilon(ku - v - b),\end{aligned} \tag{6}$$

where $\alpha = 0.139$ and $k = 0.6$ are parameters specifying the kinetics, b characterizes the asymmetry (related to the ratio of the time spent in the high- and low-value branches of the u nullcline), and $\epsilon = 10^{-3}$ is the recovery rate. We have verified that the results reported here are not sensitive to small variations in these values. Moreover, introducing different boundary conditions can yield qualitatively similar results [18].

III. RESULTS

We have carried out simulations on systems of coupled oscillators, whose individual kinetics are described by the different dynamical systems detailed in Sec. II. Despite very different expressions for $\mathcal{F}_{(p)}$ representing the intrinsic activity for each of these systems, upon coupling the oscillators exhibit strikingly similar patterns (Fig. 2). Furthermore, the broad nature of the collective dynamics does not appear to depend appreciably on the dimensionality of the lattice, or indeed, its connectivity. It is apparent from Fig. 3 that the broad trends of observing synchronized oscillations at low D_v and time-invariant, arrested states at higher D_v values hold across different model kinetics and lattice dimensions. The diversity of patterns that can be generated by these models is illustrated in Figs. 2(a) and 2(b), corresponding to spatiotemporal activity in a ring of cell-cycle oscillators (see Sec. II A) and a chemical system undergoing autocatalytic reactions that exhibits periodic activity far from equilibrium (see Sec. II B), respectively. The different patterns shown in panel (a) correspond to different arrangements of phase relations between neighboring oscillators that are seen for a broad range of system parameters. These include (i) Gradient Synchronization (GS), characterized by a monotonic change in the phase of oscillators along the array (manifested as a propagating front of activity), a special case of which is (ii) synchronized oscillations (SO) in which all oscillators are in the same phase, (iii) antiphase synchronization (APS) where the phase of neighboring oscillators differ by π, (iv) states corresponding to generalized phase synchronization, (v) chimera state (CS) comprising co-occurring oscillating and nonoscillating nodes (also referred to as "localization" [24]), and (vi) spatially patterned oscillator death (SPOD) in which the oscillators are arrested at different phases. While the term "Chimera" has been used in several different contexts when describing the emergent behavior of dynamical systems [25–29], it is used here to indicate states characterized by coexistence of regions with distinct dynamical behavior [18]. Rings comprising oscillators described by the Brusselator model shows patterns similar to those seen in Fig. 2(a), as well as more complex ones. As shown in Fig. 2(b), the latter include one or more *phase defects*, viz., a local phase relation between a set of neighboring oscillators that is distinct from the rest of the lattice, moving across the domain. These relatively exotic patterns occur over a restricted range of the parameter space and are specific to the nature of $\mathcal{F}_{(p)}$. We note that these patterns are reminiscent of the phenomenon of domain boundaries, which have been extensively studied in the context of nonlinear dissipative media [30].

Even for higher spatial dimensions, we observe that the collective dynamics of systems characterized by different relaxation oscillator models exhibit similar characteristics. Specifically, on comparing the spatiotemporal activity of two-dimensional lattices of coupled Brusselators [Fig. 2(c)] and interacting predator-prey populations described by the Rosenzweig-MacArthur model [Sec. II C, Fig. 2(d)], a common set of patterns is observed. These include higher dimensional analogues of GS (that manifest as traveling waves in the lattice), as well as generalized APS (where the phase of an oscillator at time t differs by π from that of its neighbor at $t + \delta t$, where δt is a short time delay). In both of these cases, we observe that the propagating fronts can take the form of spiral waves. For stronger diffusive couplings in both systems, we observe CS and SPOD patterns analogous to those reported above for 1D systems. This suggests that the effective lateral inhibition implemented by diffusion through the inactivation variable is the dominant factor underpinning the patterns that can be seen in these very different systems.

To investigate in detail the collective dynamical phenomena common to the systems of relaxation oscillators shown in Fig. 2 we consider a generic model of such oscillators, viz., the FitzHugh-Nagumo (FHN) model (see Sec. II D), to describe the dynamics of each node. Figure 4(a) shows the three most general patterns that can be observed in a ring of FHN oscillators, viz., GS, generalized APS and SPOD. In addition to these, the system exhibits all of the other robust patterns that are seen over a wide range of parameter values in the systems described earlier [see Figs. 2(a) and 2(b)], which can be viewed as either special cases (such as SO and APS) or combinations of the three aforementioned general patterns. For instance, CS corresponds to part of the system being in GS while the remainder converges to SPOD.

To quantitatively analyze the robustness of the observed patterns over the (D_v, b) parameter space, we have estimated the size of their respective basins of attractions from many $(\sim 10^3)$ realizations [Fig. 4(b)]. To classify the space into distinct pattern regimes we have used the following order parameters. First, SPOD and CS states are distinguished by determining the number of nodes for which the temporal variance of the activation variable, $\sigma_t^2(u_i)$ is zero. This allows us to define the number of nonoscillating cells N_{no} that is used to distinguish between SPOD ($N_{\rm no} = N$) and CS ($0 < N_{\rm no} < N$). To distinguish between states where all nodes are oscillating, including SO, APS, and GS, we obtain the time-average of the variance of the activation variable calculated over the lattice, $\langle \sigma_i^2(u) \rangle_t$, as well as the corresponding quantity for each of the two sublattices comprising alternating sites. The latter are zero for both SO and APS states, which are then distinguished by determining whether $\langle \sigma_i^2(u) \rangle_t$ is zero (SO) or not (APS). If all three time-averaged variances have finite values, the state is characterized as GS if the times at which the activation variable of different nodes reaches the peak value changes monotonically over the lattice, else it is

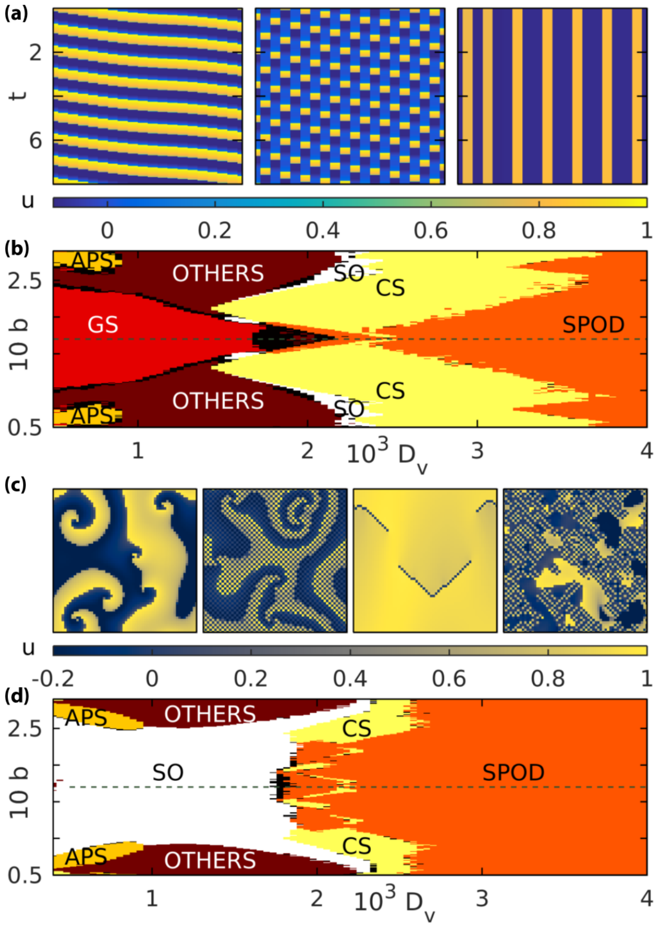

FIG. 4. Collective dynamics in lattices of coupled relaxation oscillators described by the generic FitzHugh-Nagumo (FHN) model. (a) Pseudocolor representation of the spatiotemporal evolution of the activation variable u for one-dimensional arrays showing (L-R) GS, of which SO is a special case, generalized APS and SPOD. Almost all patterns exhibited by the system, as well as those in Figs. 2(a) and 2(b), are either one of these or can be viewed as combinations thereof (e.g., CS). The system comprises $N = 20$ oscillators diffusively coupled on a ring through the inactivation variable v with strength D_v. (b) Different dynamical regimes of the above system in the (D_v, b) parameter plane, labeled by the attractor to which the majority ($> 50\%$) of initial conditions converge, viz., SO, GS, APS, CS, SPOD, and OTHERS. If a majority of initial conditions do not converge to a single attractor, then the corresponding region is shown in black. (c) Snapshots of the activation variable u in a two-dimensional array comprising $N \times N$ relaxation oscillators displaying: (L-R) a GS and a generalized APS state both exhibiting traveling fronts in the form of spiral waves, "gliders" (linelike phase defects propagating on SO background), and CS. (d) Dynamical regimes of the two-dimensional system analogous to the parameter space diagram shown in panel (b). For panels (c, d), oscillators are coupled to their four nearest neighbors on the lattice with periodic boundary conditions; for (c) $N = 60$ and (d) $N = 10$. Note that both the parameter space diagrams (b, d) exhibit reflection symmetry about $b = 0.17$ (represented by the broken horizontal line).

classified as OTHERS. Note that OTHERS includes a large number of diverse complex spatiotemporal patterns including generalized APS. In practice, the different pattern regimes are identified by specifying thresholds on the above order parameters, whose specific values do not affect the qualitative nature of the results. Parameter regions are marked as GS, SO, APS, SPOD, and CS states if they are obtained for $>50\%$ of random initial conditions (i.e., have the largest basin). We note that SO is harder to obtain in larger systems as the rapid coordination required for exact synchronization is easier to achieve in smaller systems.

A striking feature of the (D_v, b) parameter space diagram for the one-dimensional array of coupled FHN oscillators is that the three general patterns occur at either end of the coupling strength range, with SPOD being found at the higher values of D_v while in the lower range we observe GS, as well as antiphase patterns. The antiphase collective dynamics manifests itself when the individual oscillator limit cycles are highly asymmetric, corresponding to lower values of b. Indeed, in the limit of extreme asymmetry where a node remains in one of the branches (slow or fast) for almost the entire duration of its oscillation period, it can be shown analytically that APS is the only stable state for the system [18]. We would also like to note that while SPOD states resemble Turing patterns [17], the generative mechanism is quite distinct from that of Turing instability and involves the arrest of oscillators into a heterogeneous stationary state, as demonstrated in Ref. [18]. Consistent with the earlier statement that all patterns other than the three general ones (and their special cases) can be seen as combinations thereof, we observe that these patterns (such as CS) occur in the region between the GS and SPOD regimes. Observation of SO at higher values of D_v can be interpreted as a result of increased coordination resulting from stronger coupling between the oscillators.

Investigation of the spatiotemporal dynamics in two-dimensional lattices of $N \times N$ coupled FHN oscillators reveals the existence of patterns similar to those seen in Figs. 2(c) and 2(d), including spiral waves, propagating phase defects and CS [Fig. 4(c)]. The corresponding (D_v, b) parameter space [Fig. 4(d)] displays regimes corresponding to SO, APS, CS, SPOD, and OTHERS identified using methods similar to those used for 1-dimensional lattices. The strong qualitative similarity with Fig. 4(b) is visually apparent. Note that SO is seen to occur over a large region of the parameter space to the exclusion of GS as Fig. 4(d) is for a small lattice (viz., $N = 10$). For larger lattices, signals take longer to traverse the domain making global phase coherence less likely, which results in localized phase coordination manifesting as waves (i.e., GS will dominate).

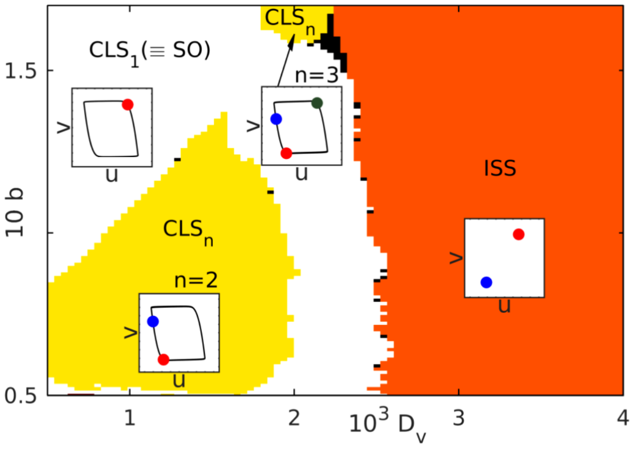

FIG. 5. Different dynamical regimes of a globally coupled system of $N(= 100)$ FHN oscillators diffusively coupled through the inactivation variable v are shown in the (D_v, b) parameter plane. This mean-field model displays two fundamental patterns of collective activity, viz., Cluster Synchronization (CLS) at low D_v and inhomogeneous steady state (ISS) at high D_v. The CLS states are further classified on the basis of the number of clusters n into which the oscillators are grouped according to their phase, e.g., CLS$_1$ which is identical to SO, CLS$_2$ which is equivalent to APS and CLS$_3$ that is seen for high b. The insets show the location of each oscillator (colored circles) on its trajectory in (u, v) phase space at a particular time instant for the dominant attractor in each regime. Note that in ISS the oscillators are arrested at low or high values, analogous to SPOD seen in lattices.

The qualitative similarity of the parameter space diagrams for one- and two-dimensional lattices [Figs. 4(b) and 4(d)] suggests that the nature of the pattern regimes seen for a system of such coupled oscillators is independent of the dimensionality. To verify this we now consider a mean-field system of globally coupled FHN oscillators which corresponds effectively to the limit of extremely large number of dimensions (Fig. 5). We observe that the parameter space is dominated by essentially two collective dynamical states, viz., Cluster Synchronization (CLS$_n$) comprising in general n oscillator clusters (each cluster being characterized by the common phase of all the constituent nodes) and the temporally invariant inhomogeneous steady state (ISS), where the dynamics of each node is arrested to one of two possible values [see inset in Fig. 5]. We would like to point out that all the observed spatiotemporal patterns mentioned earlier can be viewed as instances or combinations of these two fundamental states. In particular, ISS is equivalent to the SPOD state observed in a finite-dimensional lattice. The spatially symmetric SO state where all oscillators have the same phase, and hence belong to a single cluster, corresponds to CLS$_1$. Similarly, the spontaneously broken spatial symmetry APS state comprising two clusters of oscillators that are exactly π out of phase, belongs to CLS$_2$. We also observe other CLS$_n$ states corresponding to higher values of n in small regions of the parameter space.

Deviating from the mean-field situation by reducing the number of connections per node will result in the emergence of other robust patterns. In particular, it is possible to observe collective states where the number of clusters is equal to the total number of nodes in the system, i.e., CLS$_N$. This will correspond to GS in lattices with a finite coordination number. Its occurrence is inversely related to the communication efficiency, i.e., how rapidly signals coordinate activity across the system. This is governed by the diffusion strength, as well as, the number of connections (relative to the system size), and increasing either may result in merging of clusters that could possibly lead to the globally coherent SO (i.e., CLS$_1$) state. We would like to note that qualitatively similar results to those observed for the case $D_u = 0$ can be

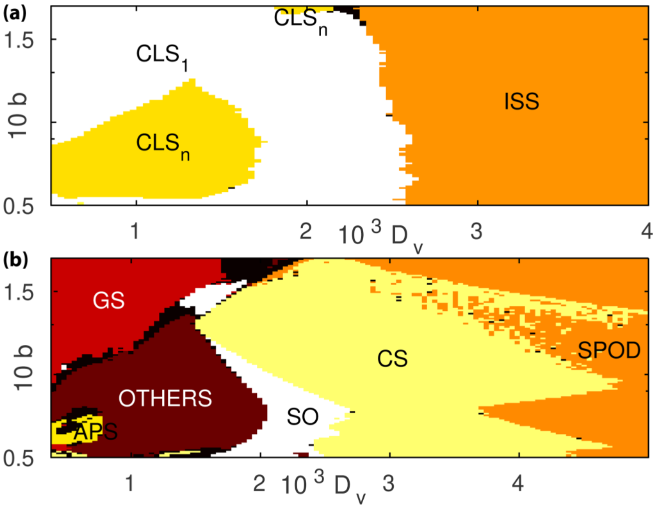

FIG. 6. Different dynamical regimes of a system of FHN oscillators, diffusively coupled through the inactivation variable v for the case $D_u = D_v$, are shown in the (D_v, b) parameter plane for (a) a globally coupled system ($N = 100$) that exhibits two fundamental patterns of collective activity, viz. Cluster Synchronization (CLS) and Inhomogeneous Steady State (ISS), and (b) a ring of size $N = 20$ that exhibits SO, GS, APS, CS, SPOD, and OTHERS. In each case, the dynamical regimes are labeled by the attractor to which the majority (>50%) of initial conditions converge.

obtained even when $D_u = D_v$, i.e., when both activation and inactivation variables are diffusively coupled with the same strength to their neighboring sites (Fig. 6).

As it is now apparent that the observed patterns in the one- and two-dimensional lattices can be understood as instances of the fundamental patterns CLS$_n$, ISS and combinations thereof, we now focus on how these two collective dynamical states compete with each other at the interface of these two regimes in the FHN parameter space. Figure 7 shows that close to this boundary the system can converge to either one of the two attractors depending on the (randomly chosen) initial condition. This convergence happens after a period of transient activity that resembles diffusion-mediated coarsening phenomena seen, e.g., in binary mixtures [31,32]. As seen in Fig. 7(a), a ring of FHN oscillators in this parameter regime exhibit the rapid creation of several domains of varying sizes, each being either in a CLS or SPOD state. Over time some of these domains expand at the expense of others in a process of competitive growth akin to Ostwald ripening [33], with the entire system eventually converging to either CLS$_n$ or SPOD states [top and bottom panels of Fig. 7(a), respectively]. The sizes of the basins of attraction for these two states can be discerned from the asymptotic probability density of $f_{\rm osc}$, viz., the fraction of nodes that belong to any of the domains exhibiting oscillations, whose time evolution is shown in Fig. 7(b). Figure 7(c) shows how, as the system approaches the asymptotic state, the number of distinct domains $n^{\rm domain}$ reduces over time through a process of coalescence. Similar coarsening phenomena leading to any of the two fundamental patterns are also seen for two-dimensional lattices of coupled oscillators [Fig. 7(d)].

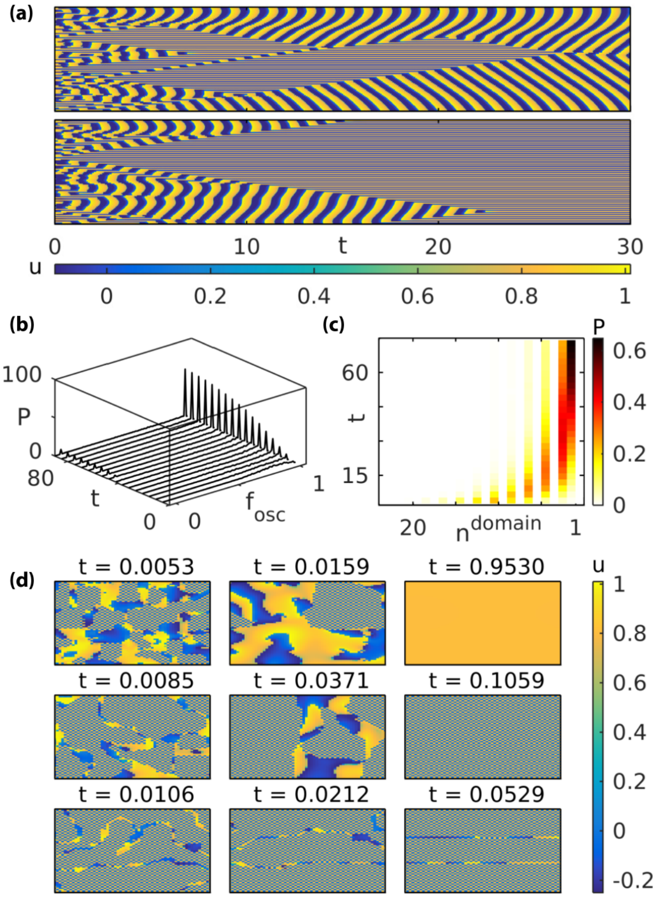

FIG. 7. Convergence of the collective dynamics of lattices of FHN oscillators to one of the fundamental attractors can be understood as a coarsening process. (a) Pseudocolor representation of the spatiotemporal evolution of the activation variable u on a ring of $N = 100$ oscillators. For the same set of parameter values ($b = 0.175$, $D_v = 1.8 \times 10^{-3}$), the system converges to either GS (top) or SPOD (bottom), depending on the random initial state. (b) The coarsening shown in panel (a) can be quantitatively represented in terms of the evolution of the Probability density function (pdf P) for $f_{\rm osc}$, the fraction of oscillating nodes at a given time. Note that asymptotically the distribution converges to an approximately bimodal form comprising two peaks around $f_{\rm osc} = 0$ (corresponding to SPOD) and $f_{\rm osc} = 1$ (corresponding to GS). The probabilities are estimated from 10^3 realizations. (c) The process of coalescence of multiple domains, each comprising either oscillating or nonoscillating nodes exclusively, is quantitatively displayed in terms of the time evolution of the pdf for the number of such domains, $n^{\rm domain}$. (d) Snapshots of u in a two dimensional array (with periodic boundary conditions) comprising $N \times N$ ($N = 60$) relaxation oscillators. For the same set of parameter values as above, the system converges to either SO (top) or SPOD (middle), depending on the initial state. It is also possible to see states where further coarsening to SPOD is arrested by the presence of line defects, comprising oscillating cells that move extremely slowly (bottom).

IV. CONCLUSION

To conclude, we have shown that a variety of similar patterns are exhibited by diverse systems having different local dynamics and connection topologies. This can be explained by noting that all of these patterns are either particular manifestations, or arise through interactions between, two fundamental classes of collective dynamical states. These are characterized either by one or more synchronized clusters, or temporally invariant inhomogeneous patterns. As we show, in general, they will arise from the collective dynamics of a system comprising relaxation oscillators that are coupled through the inactivation components, a feature that is common across the systems that we have considered here. While weak interactions typically generate CLS$_n$, stronger coupling yields ISS. This mechanism of pattern formation, distinct from the classic Turing paradigm, is sufficiently generic to have been observed in experimentally realizable settings, such as in coupled electronic circuits [34]. This opens up the possibility of exploring applications for the dynamics reported here, e.g., in the context of computation [35]. While we have focused exclusively on spatially extended lattice systems, it is intriguing to ask whether analogous results will be obtained for the continuum counterparts of these systems, described for instance by coupled partial differential equations of the reaction-diffusion type. It will also be of interest to extend the investigation beyond the systems of relaxation oscillators (comprising components whose dynamical evolution involve very different timescales) that have been considered here and to study, for example, diffusively coupled Stuart-Landau oscillators. In the continuum limit, such a system is described by the complex Ginzburg-Landau equation [36] that is known to exhibit a wide range of complex spatiotemporal behavior [37]. Finally, as diffusion is not the only mechanism through which the dynamical components of a spatially extended system interact, it will be of interest to see how the introduction of other processes, such as advection, will affect the nature of the spatiotemporal patterns generated by such systems. This will, for example, be relevant in the context of predator-prey systems embedded in environments subject to hydrodynamic flows [38] (e.g., oceanic plankton populations [39,40]).

ACKNOWLEDGMENTS

R.J. is supported by IMSc Project of Interdisciplinary Science and Modeling (PRISM), and S.N.M. is supported by IMSc Complex Systems Project (XII Plan), both funded by the Department of Atomic Energy, Government of India. R.J. thanks A. S. Vytheeswaran and the Department of Theoretical Physics, University of Madras, for their support. The simulations required for this work were done in the IMSc High Performance Computing facility (Nandadevi, Annapurna and Satpura clusters). The Satpura cluster is partly funded by the Department of Science and Technology, Government of India (Grant No. SR/NM/NS-44/2009) and the Nandadevi cluster is partly funded by the IT Research Academy (ITRA) under the Ministry of Electronics and Information Technology (MeitY), Government of India (ITRA-Mobile Grant No. ITRA/15(60)/DIT NMD/01). We thank Bulbul Chakraborty, Pranay Goel, Chittaranjan Hens, Sandhya Koushika, Sandeep Krishna, Tanmay Mitra, Prasad Perlekar, and Soling Zimik for helpful discussions.

[1] M. C. Cross and P. C. Hohenberg, Rev. Mod. Phys. **65**, 851 (1993).

[2] P. Ball, *The Self-Made Tapestry: Pattern Formation in Nature* (Oxford University Press, Oxford, 2001).

[3] S. Sinha and S. Sridhar, *Patterns in Excitable Media* (CRC Press, Boca Raton, FL, 2015).

[4] G. Buzsáki and A. Draguhn, Science **304**, 1926 (2004).

[5] P. Lenz and L. Søgaard-Andersen, Nat. Rev. Microbiol. **9**, 565 (2011).

[6] L. Potvin-Trottier, N. D. Lord, G. Vinnicombe, and J. Paulsson, Nature (London) **538**, 514 (2016).

[7] M. Guzzo *et al.*, Nature Microbiol. **3**, 948 (2018).

[8] E. M. Izhikevich, SIAM J. Appl. Math. **60**, 1789 (2000).

[9] L. Glass, Nature (London) **410**, 277 (2001).

[10] A. Pikovsky, M. Rosenblum, and J. Kurths, *Synchronization* (Cambridge University Press, Cambridge, 2001).

[11] H. Meinhardt and A. Gierer, J. Cell Sci. **15**, 321 (1974).

[12] P. W. Sternberg, Nature **335**, 551 (1988).

[13] J. R. Collier, N. A. M. Monk, P. K. Maini, and J. H. Lewis, J. Theor. Biol **183**, 429 (1996).

[14] N. Li, N. Tompkins, H. O. González-Ochoa, and S. Fraden, Eur. Phys. J. E **38**, 18 (2015).

[15] P. Turchin, *Complex Population Dynamics* (Princeton University Press, Princeton, NJ, 2003).

[16] M. Toiya, V. K. Vanag, and I. R. Epstein, Angew. Chem. **47**, 7753 (2008).

[17] A. M. Turing, Phil. Trans. Roy. Soc. Lond. B **237**, 37 (1952).

[18] R. Singh and S. Sinha, Phys. Rev. E **87**, 012907 (2013).

[19] J. E. Ferrell, T. Y. Tsai, and Q. Yang, Cell **144**, 874 (2011).

[20] I. Prigogine and R. Lefever, J. Chem. Phys. **48**, 1695 (1968).

[21] A. M. Zhabotinsky, Chaos **1**, 379 (1991).

[22] M. L. Rosenzweig and R. H. MacArthur, Am. Nat. **97**, 209 (1963); M. L. Rosenzweig, Science **171**, 385 (1971).

[23] R. Fitzhugh, Biophys. J. **1**, 445 (1961); J. Nagumo, S. Arimoto, and S. Yoshizawa, Proc. IRE **50**, 2061 (1962).

[24] V. K. Vanag and I. R. Epstein, Chaos **17**, 037110 (2007).

[25] H. G. Rothstein, N. Kopell, A. M. Zhabotinsky, and I. R. Epstein, SIAM J. Appl. Math **63**, 1998 (2003).

[26] D. M. Abrams and S. H. Strogatz, Phys. Rev. Lett. **93**, 174102 (2004).

[27] D. M. Abrams, R. Mirollo, S. H. Strogatz, and D. A. Wiley, Phys. Rev. Lett. **101**, 084103 (2008).

[28] R. Singh, S. Dasgupta, and S. Sinha, Europhys. Lett. **95**, 10004 (2011).

[29] I. F. P. Kemeth, S. W. Haugland, L. Schmidt, I.G. Kevrekidis, and K. Krischer, Chaos **26**, 094815 (2016).

[30] B. A. Malomed, A. A. Nepomnyashchy, and M. I. Tribelsky, Phys. Rev. A **42**, 7244 (1990).

[31] J. M. Wen, J. W. Evans, M. C. Bartelt, J. W. Burnett, and P. A. Thiel, Phys. Rev. Lett. **76**, 652 (1996).

[32] T. Mullin, Phys. Rev. Lett. **84**, 4741 (2000).

[33] L. Raatke and P. W. Voorhees, *Growth and Coarsening* (Springer, Berlin, 2002).

[34] L. V. Gambuzza, A. Buscarino, S. Chessari, L. Fortuna, R. Meucci, and M. Frasca, Phys. Rev. E **90**, 032905 (2014).

[35] S. N. Menon and S. Sinha, in *Proceedings of the 2014 International Conference on Signal Processing and Communications (SPCOM)* (IEEE, Bangalore, India, 2014), p. 1.

[36] V. García-Morales and K. Krischer, Contemp. Phys. **53**, 79 (2012).

[37] I. S. Aranson and L. Kramer, Rev. Mod. Phys **74**, 99 (2002).

[38] Z. Neufeld, Phys. Rev. Lett. **87**, 108301 (2001).

[39] E. R. Abraham, Nature **391**, 577 (1998).

[40] Z. Neufeld, P. H. Haynes, V. Garçon, and J. Sudre, Geophys. Res. Lett. **29**, 1534 (2002).